ACS Sustainable Chemistry & Engineering

pubs.acs.org/journal/ascecg

Research Article

Enhanced Stability and Photochemical Activity of Photosystem I from the Green Alga *Chlamydomonas reinhardtii* Upon Encapsulation in Organic Matrixes

Salvatore C. Gaglio,[#] Giorgia Zanella,[#] Stefano Cazzaniga, Nico Olivieri, Elia Battagini, Alessandro Romeo, Matteo Ballottari,* and Massimiliano Perduca*

Cite This: *ACS Sustainable Chem. Eng.* 2025, 13, 5046−5056

Read Online

ACCESS | Metrics & More | Article Recommendations | Supporting Information

ABSTRACT: Photosynthesis is a fundamental process that converts light energy into chemical energy, driven by photosystems. These chlorophyll-protein complexes enable a light-dependent electron transport chain, producing ATP and NADPH, which are essential for carbon fixation. Photosystem I (PSI), well-known for its greater photochemical performance and stability, has been utilized in hybrid nanodevices as a light converter and photocatalyst. However, membrane proteins, including PSI, often suffer from stability loss and decreased activity following purification due to their removal from the thylakoid membrane environment. To address these challenges, isolated PSI from *Chlamydomonas reinhardtii* was encapsulated into different biodegradable polymers, including poly lactic co-glycolic acid (PLGA), poly lactic acid (PLA), and chitosan (Ch), using double emulsion and ionic gelation methods, and stable PSI nanoparticles (100−500 nm) with tailored surface charges were produced. These matrices provide a stabilizing shell mimicking the natural environment, enhancing PSI stability and activity under different conditions of both temperature and pH. Herein, reported results demonstrate that encapsulated PSI maintains higher photochemical activity over time compared to detergent-stabilized PSI, with chitosan showing the highest efficiency in preserving PSI activity under strong light and extended periods. Remarkably, the encapsulated PSI retained activity up to 7−8 times greater over 28 days compared to the same complex stabilized in detergents. Finally, encapsulation offers enhanced stability and activity, leveraging the advantages of the microalgae in sustainable biomass production over land plants. This work paves way for environmentally friendly and efficient photocatalytic systems integrating photosynthetic components.

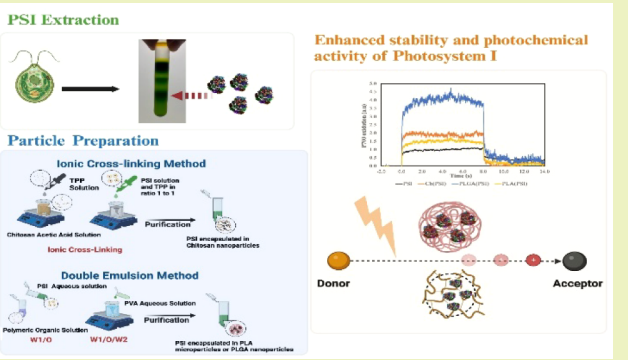

KEYWORDS: *photochemistry, photosynthesis, nanoparticles, chitosan, poly lactic-co-glycolic acid, poly lactic acid*

INTRODUCTION

Photosynthesis is a fundamental process that converts photons into chemical energy, driven by chlorophyll-protein complexes called photosystems (PS), which promote a light-dependent electron transport across the photosynthetic membranes.[1,2] In oxygenic photosynthetic organisms, two types of PS are present: photosystem I (PSI) and photosystem II (PSII), working in series to transfer electrons from the water−oxygen couple (+820 mV) via a chain of redox reactions to $NADP^+$/NADPH (−320 mV).[3−5] The reaction centers where the photochemical reactions occur comprise, as the primary electron donor, the chlorophyll dimers called P700 and P680 for PSI and PSII, respectively.

Briefly, photosynthesis begins with a light-driven charge separation at the level of P680 and P700, which generates electron transport to plastoquinone, being reduced to plastoquinol, and to ferredoxin, respectively. Reduction of $P680^+$ occurs starting from water splitting by a $CaMn_4$ cluster bound to PSII protein subunits called the oxygen-evolving complex (OEC). These electrons are used to reduce certain tyrosine residues, which in turn reduce $P680^+$ to P680. Plastoquinol transports the derived electrons to another protein complex present in the thylakoid membrane called cytochrome b6f (cytb6f), which oxidizes plastoquinol back to plastoquinone and reduces a water-soluble protein, plastocyanin, present in the lumen. At the level of PSI, the oxidized $P700^+$ is then reduced by oxidizing plastocyanin. Finally, ferredoxin is used by ferredoxin-$NADP^+$ reductase (FNR) to reduce $NADP^+$ to NADPH.[4] This light-driven electron

Received: December 18, 2024
Revised: March 7, 2025
Accepted: March 13, 2025
Published: March 24, 2025

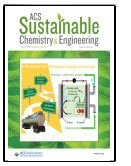

transport chain is coupled with proton transport from the stroma to the lumen, where additional protons are released due to water splitting, generating a proton gradient, which is exploited by ATP synthase to produce ATP. ATP and NADPH are then essential for fueling the carbon-fixing reactions.

Due to its higher photochemical performance and stability compared to PSII, isolated PSI has already been employed as a light converter[6−8] for the generation of current and as a photocatalyst in ex vivo redox reactions[9,10] through the assembly of hybrid nano/microarchitectures. For instance, Izzo et al.[6] designed a graphene monolayer (SLG) covered by PSI, showing a significantly improved overall photocurrent output compared to the abiotic FTO/SLG material. As a photocatalyst, PSI extracted from cyanobacteria was conjugated with PSII on gold nanoparticles, paving way for a new light-driven water-splitting nanodevice with potential use in hydrogen production.[10]

As a biological system, PSI could suffer from the phenomenon of degradation over time, leading to a loss of activity. Thus, to preserve the photochemical performance, PSI must be stabilized and protected by the environment before being integrated into hybrid nano/micro devices.[11,12] A promising approach has emerged through encapsulation technologies.[13−17] For instance, encapsulation of PSI in dry trehalose glasses resulted in improved stability of the complex, albeit with an impairment of PSI protein dynamics.[18] In addition, organic micro- and nanoparticles are able to mimic cellular membranes and organelles,[13,19,20] a crucial property for designing an environmentally friendly photocatalytic system suitable for membrane proteins like photosystems. Several previous studies reported the application of PSI in extracellular environments, coupled with different nanostructures as carbon nanotubes,[21] metal-based nanowires,[22] and plasmonic nanostructures[23−25] or embedded in conductive polymers[26,27] or biohybrid electronic devices.[28−30]

Cherubin et al.[13] demonstrated the preservation of photochemical activity when PSI isolated from spinach leaves was encapsulated into biopolymeric microparticles. In this previous work, PSI complexes were embedded in organic matrixes using PLGA (poly lactic-co-glycolic acid) polymers, forming microparticles. The PSI complexes in PLGA microparticles were characterized by increased photochemical efficiencies compared to PSI in a detergent solution and exhibited enhanced stability over time. Moreover, encapsulated PSI complexes were able to catalyze light-dependent redox reactions with electron acceptors and donors outside the PLGA microparticles.

Following this trend line, in this work, PSI encapsulation into an organic matrix was further developed, isolating this protein complex from microalgae. The possibility of obtaining photochemically active PSI from microalgae presents several potential advantages compared to the case of land plants, as discussed in the following. Microalgae have the advantage of being cultivated in industrial systems with high biomass productivity and a reduced water and carbon footprint compared to land plants.[31] Moreover, in the case of microalgae, all the biomass produced is photosynthetically active, accumulating PSI and PSII, while in the case of land plants, the photosynthetically active tissues are only a fraction of the overall biomass produced.

Here, PSI isolated from the microalgal species *Chlamydomonas reinhardtii*, a model organism for green algae, was encapsulated into poly lactic coglycolic acid (PLGA), poly lactic acid (PLA), and chitosan (Ch) particles. Due to their biocompatibility and biodegradability, PLGA, PLA, and Ch polymers have been classified as safe for human health by both the European Medicines Agency (EMA) and the U.S. Food and Drug Administration (FDA).[17,32−35] PLA is a bioderived thermoplastic with a semicrystalline composition, which makes this polymer suitable for long-term applications in the packaging or medical devices industry.[36] On the contrary, PLGA is a copolymer mostly used in drug delivery applications, where the glycolic moiety influences water erosion sensitivity, allowing for the release pattern.[32,37,38] Chitosan, a cationic amino polysaccharide derived from chitin through alkaline or enzymatic partial deacetylation, has gained attention in light-to-electron conversion applications due to its unique chemical properties.[39] These include high surface charge, biocompatibility, and the ability to support functionalization, making it suitable for stabilizing photosystems in hybrid systems for photocatalysis and artificial photosynthesis.[13] Several studies have demonstrated the use of chitosan in stabilizing photosynthetic complexes like PSI to enhance their photochemical stability and photocurrent generation in hybrid assemblies.[40] Moreover, data show its potential in assembling nanostructures that improve charge separation and transfer, enabling efficient energy conversion.[41] Another advantage is represented by the surface properties of these biopolymers, which can be easily modified to conjugate additional functional molecules or facilitate their immobilization on a supporting structure.[42−45]

Thus, using the double emulsion method and the ionic gelation technique, we were able to obtain stable and efficient photocatalytic hybrid nano and microparticles (100−500 nm) showing different surface charges and properties.

MATERIALS AND METHODS

Cultivation of Microalgae. *C. reinhardtii* strain adopted herein is CC-125 mt$^+$. Algal cells were cultivated in Tris-acetate-phosphate (TAP)[46] and liquid cultures were maintained in shake flasks at 25 °C under 70−100 μmol photons m^{-2}s^{-1} of continuous white light. Harvesting was performed at the end of the exponential phase, when the cells reached a density of 2 × 10^7 cells/mL, typically after 7 days of cultivation.

Thylakoid Extraction. Photosystem I was purified from *Chlamydomonas reinhardtii*. Briefly, microalgae were kept in the dark under shaking for 1 h and then centrifuged at 1,500 g for 5 min at 4 °C, and the pellet was resuspended in a solution containing 20 mM HEPES (pH 7.5), 5 mM $MgCl_2$, 0.3 M sucrose, and 0.5% BSA and then subjected to sonication cycles on ice (3 cycles, 30 s per cycle) to destroy the cell wall by using the BANDELIN SONOPULS HD 2070 system (BANDELIN electronic GmbH & Co. KG, Germany). The obtained eluate was centrifuged at 1,000 g for 4 min to remove intact cells from the solution. Subsequently, thylakoids were purified from the supernatant through three serial centrifugations (6,000, 8,000, and 10,000 g for 15 min each). Finally, the samples were resuspended in a buffer containing 50% (w/v) glycerol, 20 mM HEPES (pH 7.5), and 5 mM $MgCl_2$ to protect thylakoids from freezing in liquid nitrogen and were stored at −80 °C.

Photosystem I Isolation. Isolated thylakoids, corresponding to 600 μg of chlorophyll, were centrifuged (15 min at 21,000 g), and the pellet was resuspended in 1.5 mL of 10 mM EDTA (ethylenediaminetetraacetic acid) and 10 mM Hepes, pH 7.5. After keeping the samples on ice for 10 min, another centrifugation cycle was performed, and the pellet was resuspended in 1.2 mL of 10 mM Hepes, pH 7.5, and 1% dodecyl β-D-maltoside (β-DM), allowing the solubilization of thylakoids and PSI extraction through micelle formation. The solubilized membranes were loaded onto a sucrose gradient to separate the different pigment-binding complexes by

https://doi.org/10.1021/acssuschemeng.4c10593
ACS Sustainable Chem. Eng. 2025, 13, 5046−5056

ultracentrifugation (40,000 g for 20 h), as shown in Figure S1. Isolated PSI was kept in 0.5 M sucrose, 10 mM Hepes, pH 7.5, and 0.03% dodecyl β-DM; this buffer was also adopted for all the PSI measurements in detergent conditions, preserving PSI activity in the aqueous environment.

Particle Preparation: Chitosan Nanoparticles. PSI of*Chlamydomonas reinhardtii* has been encapsulated in chitosan nanoparticles (Ch NPs) by using a modified ionic cross-linking method (Figure S2).[13] Low molecular weight chitosan (Sigma-Aldrich, CAS 9012−76−4; MW 50−190 kDa), obtained from the deacetylation of chitin (from the shrimp*Pandalus borealis*), with a degree of residual acetylation corresponding to 16%, was dissolved to a final concentration of 0.1% in 0.2% acetic acid solution (pH 4.7) for 1 h to ensure complete solubilization. The resulting polymer solution was then filtered using a 0.45 μm filter to eventually remove any remaining aggregates. 1 mL of Tripolyphosphate (TPP), as the cross-linker, was added to 4 mL of the polymer solution under stirring; subsequently, an additional milliliter, consisting of a PSI solution (50 μg Chl) and TPP in a 1:1 (v/v) ratio, was added to achieve a final volume of 6 mL. Although nanoparticles formed immediately after the addition of the cross-linker, the colloidal suspension was left under stirring for 30 min to stabilize the colloidal formation. Finally, chitosan-PSI-loaded nanoparticles were collected by centrifugation (15,557 g for 20 min), washed several times with Milli-Q water, and resuspended in the desired buffer or lyophilized.

Preparation of Particles: PLGA and PLA Nano- and Microparticles. PLGA (poly[DL-lactide-co-glycolide] 50:50 lactide-glycolide ratio, Sigma-Aldrich, CAS 26780−50−7) and PLA (poly[2-hydroxypropionic acid], Sigma-Aldrich, CAS 26100−51−6) were prepared using the double emulsion method (Figure S3).[13,47,48] A solution of PSI in 0.5 M sucrose, 10 mM HEPES at pH 7.5, and 0.03% dodecyl β-DM was diluted in water (w_1) to a final quantity of 50 μg of chlorophylls as the first aqueous phase, while the polymer was dissolved in DMSO to form the organic phase (o) with a final concentration of 10 mg/mL. The first emulsion (w_1/o) was prepared by mixing 500 μL of the PSI solution with 500 μL of the polymeric solution. The second emulsion was obtained under stirring by adding the first emulsion (w_1/o) dropwise to an aqueous phase of 1% PVA (poly[vinyl alcohol], Sigma-Aldrich, CAS 9002−89−5) (w_2) as the stabilizer to obtain uniform dispersions. Finally, the obtained double emulsion (w_1/o/w_2) was left under stirring overnight to stabilize the system, enhancing nanoparticle nucleation by displacement of the organic solvent.[49] At the end, PLGA (or PLA) PSI-loaded nanoparticles were collected by centrifugation (15,557 g for 20 min), washed several times with Milli-Q water, and resuspended in the final buffer or lyophilized. Empty nanoparticles were prepared using the same protocol, avoiding the presence of PSI in the first aqueous phase.

Dynamic Light Scattering (DLS). Particle size and ζ-potential were estimated by dynamic light scattering (DLS) (Nano ZetaSizer ZS, ZEN3600, Malvern Instruments, Malvern, Worcestershire, U.K.), by measuring the Brownian motion of the particles and using the Stokes−Einstein equation to calculate the hydrodynamic diameter of the particles,[50] as well as by measuring the surface charge of the particles. This latter parameter can be used to predict the stability of the dispersion.[51] All the samples were resuspended and diluted 1:20 in Milli-Q water before performing the analysis at a constant temperature of 25 °C.

Nano Tracking Analysis (NTA). To further support DLS size results, Nano tracking analysis was performed using the NanoSight (Malvern NanoSight NS300, Malvern Panalytical Ltd., Malvern, UK). NTA measures the Brownian motion of the particles and uses the Stokes−Einstein equation to calculate their hydrodynamic diameter, providing a high-resolution size distribution of the particles in the sample.[52] Due to the high concentration of particles, each sample was diluted 100 times in Milli-Q water. A total of 1,498 frames, divided into 3 runs of 60 seconds each, were recorded at a camera level of 13, and the analysis was performed with a detection threshold in the range of 3−5. Finally, the number of particles per milliliter was estimated as well.

Atomic Force Microscopy. Twenty μL of each sample (prepared as described in the above section) were loaded onto a bracket covered with an inert mica surface. After 20 minutes of solvent evaporation, the analysis was performed using an NT-MDT Solver Pro atomic force microscope (Moscow, Russia) with an NT-MDT NSG01 gold-coated silicon tip in semi-contact mode with different scanning frequencies (3−1 Hz) to produce optimized AFM images.[53] The microscope was calibrated using a calibration grating (TGQ1 from NT-MDT) in order to reduce nonlinearity and hysteresis in the measurements. Finally, images were processed with the Scanning Probe Image Processor (SPIP) program (Image Metrology ApS, version 5.13, Lyngby, Denmark), and a statistical study was performed to compare the AFM diameter to DLS and Nanosight size distribution.

Absorbance Analysis and Chlorophyll Quantification. The absorption spectra of PSI in detergent or embedded within different biopolymers were registered between 350 and 750 nm and corrected for scattering. Chl exhibits two absorption bands in the blue and red regions, known as the Soret band and the Qy band, respectively.[54] Chl concentration was quantified upon extraction in DMSO, followed by dilution at a ratio of 1:10 (v/v) in acetone 80%. The absorption spectra of the pigment extracts in the visible region were then measured and fitted with the different pigment absorption spectral forms to determine the Chl concentration.[55] For rapid estimation of the Chl concentration in PSI samples, a conversion factor of 0.0162 μg [Chl]/OD was adopted, where the Chl concentration is expressed as μg/μL and OD is the maximum optical density in the Qy band (around 680 nm). This conversion factor was calculated from PSI in detergent solution.

Encapsulation Efficiency. The encapsulation efficiency (EE) was expressed in terms of Chl content by applying the following equation:

$$\mathrm{EE}\ (\%) = \frac{\mu g\ \mathrm{Chl}_{\mathrm{loaded}}}{\mu g\ \mathrm{Chl}_{\mathrm{fed}}} \times 100$$

where $\mathrm{Chl}_{\mathrm{loaded}}$ refers to the chlorophyll content inside the nanoparticles, and $\mathrm{Chl}_{\mathrm{fed}}$ is the chlorophyll amount measured for the PSI used during the encapsulation process.

P700 Oxidation Kinetic. PSI photochemical activity was assessed by following the protocol described by Cherubin et al.[13] Briefly, P700 oxidation upon actinic light illumination was analyzed by measuring pump−probe transient absorption at 830 nm minus the reference signal at 870 nm by using the Dual Pam-100 (WALZ Photosystem Instruments). P700 oxidation kinetics were measured for free PSI in detergent (0.5 M sucrose, 10 mM HEPES, pH 7.5, and 0.03% dodecyl β-D-maltoside) and PSI-carrying polymeric particles resuspended in different buffers by applying an actinic red light of 940 $\mu mol \cdot m^{-2} \cdot s^{-1}$. Furthermore, ascorbate and methyl-viologen, the electron donor and acceptor, respectively, were added to the samples at a concentration of 1 mM. Further, PSI activity, both alone and embedded within polymeric particles, was studied over time, at different temperatures, and under intense light (1,500 $\mu mol\ m^{-2}\ s^{-1}$) to evaluate its stability. Electron transfer reactions with external electron donors and acceptors were performed as previously described Cherubin et al.[13] using 1 mM0 μM methylene blue, respectively, illuminating with an actinic blue light of 100 $\mu mol \cdot m^{-2} \cdot s^{-1}$. Methylene blue reduction was then monitored by measuring absorption in the 570−700 nm region.

SDS-PAGE. Sodium dodecyl sulfate−polyacrylamide gel electrophoresis (SDS-PAGE) was performed by using a Mini-PROTEAN gel system (BIO-RAD, USA). In the case of PSI embedded in PLA or PLGA, the nanoparticles were disassembled with DMSO 100%; the samples were then centrifuged (20,000 g for 10 min), and the supernatant was discarded. In the case of PSI in Ch, the nanoparticles were first treated with acetic acid (0.2%) and then with DMSO, as in the case of samples in PLA or PLGA. Protein extracts were then incubated for 1 h at room temperature in the presence of 125 mM Tris-HCl, pH 6.8, 3.5% (w/v) sodium dodecyl sulfate (SDS), 10% (w/v) glycerol, 2 M urea, and 5% β-mercaptoethanol. PSI in detergent or intact thylakoids were immediately treated with the SDS-containing solution and incubated for 1 h. The samples were then

https://doi.org/10.1021/acssuschemeng.4c10593
ACS Sustainable Chem. Eng. 2025, 13, 5046−5056

Table 1. DLS, NTA, and AFM Data for Empty and Loaded Particles

Sample	Size[a] (nm)	PDI[b]	NTA mode[c] (nm)	AFM diameter[d] (nm)
Empty Ch	232.8 ± 77.5	0.337 ± 0.033	231.1 ± 67.2	199.4 ± 17.9
Empty PLGA	117.0 ± 37.6	0.073 ± 0.006	110.0 ± 42.9	205.7 ± 42.6
Empty PLA	470.6 ± 76.5	0.422 ± 0.098	188.6 ± 80.6	536.8 ± 98.6
Ch(PSI)	271.6 ± 70.9	0.280 ± 0.023	236.7 ± 63.3	260.9 ± 40.8
PLGA(PSI)	184.5 ± 58.8	0.120 ± 0.021	171.5 ± 52.7	242.8 ± 44.9
PLA(PSI)	491.1 ± 86.53	0.502 ± 0.098	273.7 ± 93.7	495.6 ± 88.9

[a]Size is described as the peak number collected with DLS. [b]PDI is the Poly Disperse Index. [c]NTA mode represents the tendency of NTA average size distribution. [d]AFM diameter was calculated considering particle populations greater than 100 units.

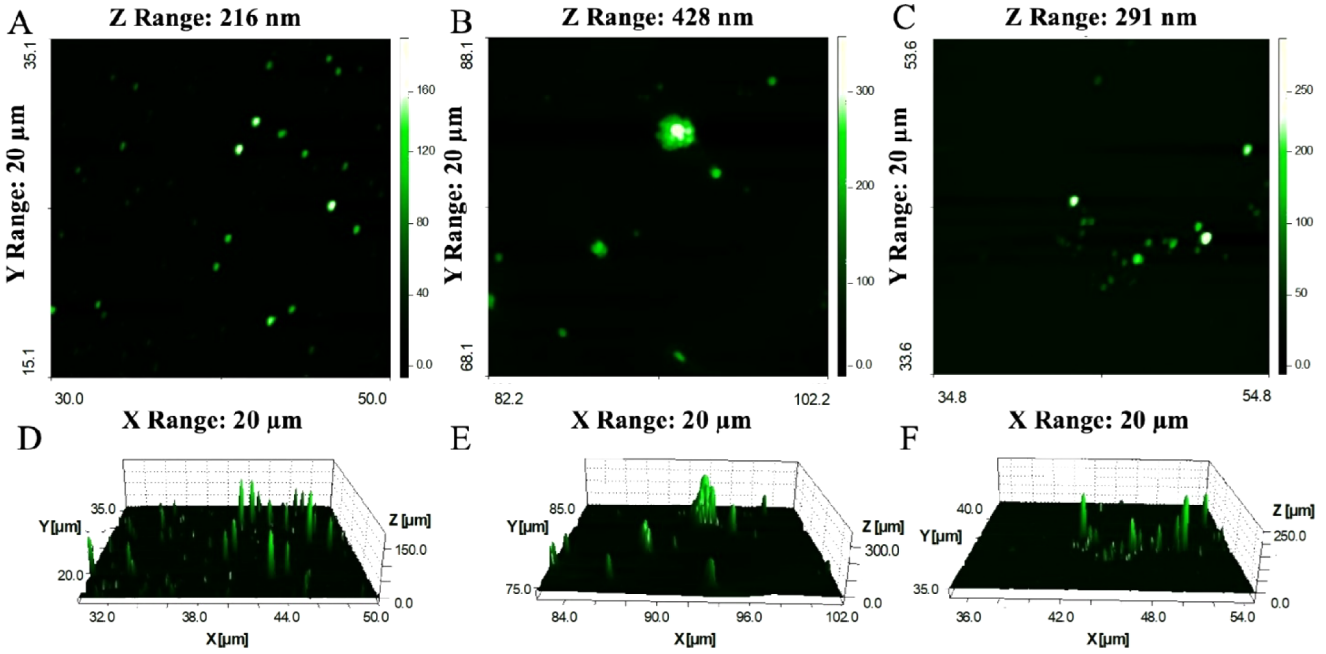

Figure 1. Atomic force microscopy data, 2D and 3D images, of PSI embedded in PLGA (A,D), PLA (B,E), and Ch (C,F), microparticles. The images have been acquired in dry mode.

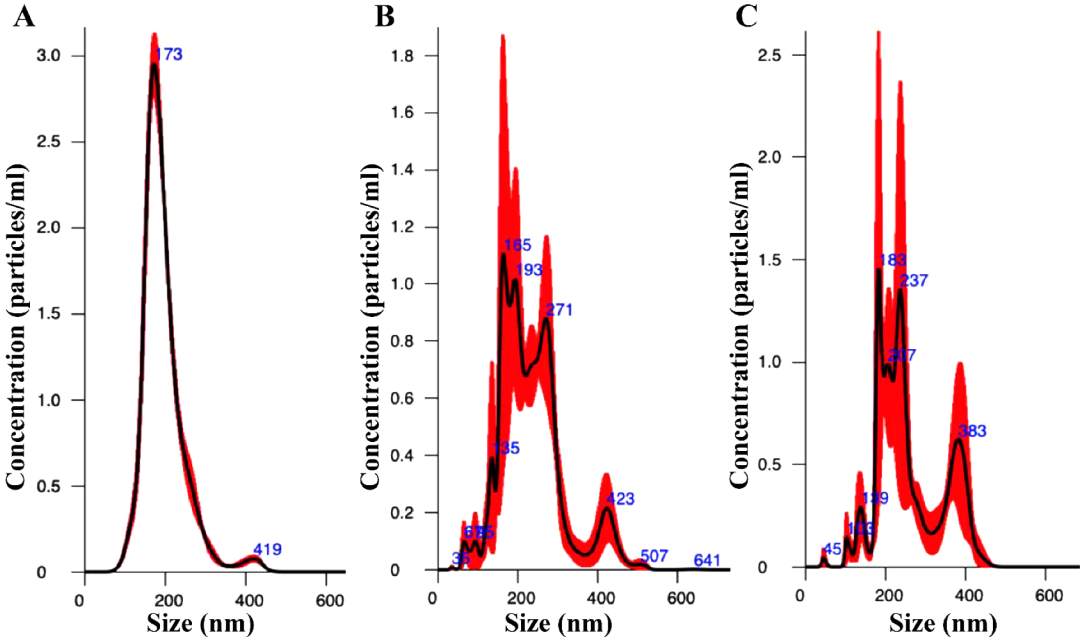

Figure 2. Size distribution of PSI embedded in PLGA (A), PLA (B), and Ch (C), collected with NTA analysis.

https://doi.org/10.1021/acssuschemeng.4c10593
ACS Sustainable Chem. Eng. 2025, 13, 5046−5056

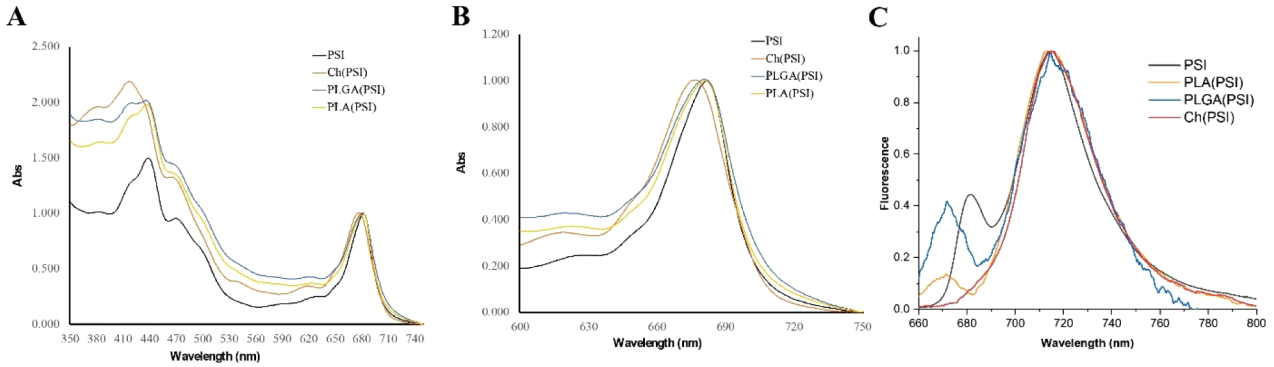

Figure 3. (A) Absorption spectra of PSI in detergent (black line) and embedded with PLGA (blue line) and PLA (yellow line) and chitosan (orange line) biopolymers. (B) Absorption spectra in the range 600−750. (C) 77K Fluorescence emission of PSI in detergent or in organic matrixes measured upon excitation at 475 nm. All samples were normalized to 1 in the red region at the maximum absorbance of PSI of approximately 680 nm.

centrifuged (20,000 g for 5 min) and subsequently loaded into the SDS-PAGE gel. Staining was performed with Coomassie blue.

77k Fluorescence. 77K fluorescence emission was measured using a BeamBio custom device equipped with a USB2000+ OceanOptics spectrometer and custom LED light sources for excitation at 475 nm.

Statistical Analysis. All the synthesis and measurements reported in this work were performed in three independent replicates, with three technical replicates each. Error bars are reported as the standard deviation. Statistical significance is expressed by different letters according to the Tukey−Kramer test (n = 3).

Data and Material Availability. All of the data and materials generated and/or analyzed during the current study are available from the corresponding authors upon reasonable request.

RESULTS

PSI Encapsulation and Physicochemical Characterization. PSI was purified from *Chlamydomonas reinhardtii* cells and encapsulated in nanosized particles (Figure S4) following two different protocols. Unlike previous studies, where the modified solvent displacement (MSD) method led to the formation of microparticles,[13] herein, a double emulsion approach was used to prepare both loaded and unloaded PLGA and PLA particles, successfully achieving nanosized dimensions. For chitosan particle preparation, the reduced dimensions were achieved by modifying the ionic-gelation protocol used in previous work.[13] Size distribution was analyzed using three different methods: DLS, NTA, and AFM, as shown in Table 1. PLGA nanoparticles showed the smallest size values, 117.0 ± 37.6 and 184.5 ± 58.8 nm for empty and PSI-loaded particles , respectively, while the largest size values were obtained with PLA (470.6 ± 76.5 and 491.1 ± 86.53 nm). Chitosan led to the production of nanoparticles with intermediate values of 232.8 ± 77.5 and 271.6 ± 70.9 nm. Figure 1 shows AFM images (in 2D and 3D) in which PSI-bearing particles appear round shaped. Moreover, the PDI value (0.120 ± 0.021) of PLGA(PSI) NPs suggests a monodispersed population, as confirmed by the NTA size distribution profile (Figure 2B) and by the isolated nanoparticles in the AFM image (Figure 1B). In the case of PLA and Ch AFM images (Figure 1A,C), the tendency to aggregate increases, leading to a polydisperse trend in the NTA size distribution (PLA > Ch) (Figure 2A, C). Furthermore, the PDI values of PLA (PSI) and Ch (PSI), 0.502 ± 0.098 and 0.280 ± 0.023, respectively, were higher than those obtained with PLGA. Ch and PLA empty particles show size and PDI values close to the loaded ones, while a general increase was observed for PLGA when PSI was encapsulated.

To study the colloidal stability, ζ-potential (mV) analysis was performed for each particle formulation (Table S1). Positive values were collected for Ch-based nanoparticles: the empty ones showed a ζ-potential of +24.6 ± 1.2 mV, while in the presence of PSI, a reduction in the surface charge was observed (+17.2 ± 1.49 mV). The same trend in ζ-potential was observed for the negative PLGA nanoformulations, where empty and loaded nanoparticles exhibited potentials of −9.1 ± 0.95 mV and −4.9 ± 0.87 mV, respectively. Surface charge did not change when PSI was encapsulated into PLA; empty PLA and PLA(PSI) showed potentials of −2.1 ± 0.2 mV and −2.4 ± 0.5 mV, respectively.

The presence of PSI was assessed using UV−vis spectroscopy analysis. Figure 3 shows the absorption spectra (350−750 nm) of the different nanoformulations, where a peak is evident at 660−680 nm, typical of chlorophyll absorption (Figure 3A). Compared to PSI in detergent solution, the nanoformulations were characterized by scattering, which is especially noticeable at lower wavelengths. The presence of scattering is consistent with the physicochemical structure of nanoparticles. When the absorption spectra were normalized to the maximum absorption in the 600−750 nm region, broader peaks in the 600−750 nm region were observed in the case of nanoassemblies compared to PSI in detergent, indicating the formation of stronger Chl-Chl interactions when PSI was embedded in an organic matrix, likely due to protein aggregation. A peculiar case is PSI embedded in a chitosan matrix, Ch(PSI), which was characterized by a blueshift in the absorption spectrum, consistent with previous data obtained for PSI isolated from spinach leaves.[13] When fluorescence emission was measured at 77K, all PSI samples exhibited a maximum peak at 715 nm, but the samples in organic matrixes were characterized by a broadening of the emission spectrum with increased emission at longer wavelengths, consistent with the presence of stronger Chl-Chl interactions In the case of PSI in detergent or in PLA or PLGA polymers, an additional peak in the 77K fluorescence emission spectrum in the 650−690 nm region was related to the presence of some antenna proteins (680 nm maximum emission) or free chlorophylls (670 nm maximum emission) disconnected from the PSI complex. The presence of free antenna proteins or free Chl is commonly observed in PSI preparations, representing a minor component but with a high fluorescence quantum yield.[56,57]

https://doi.org/10.1021/acssuschemeng.4c10593
ACS Sustainable Chem. Eng. 2025, 13, 5046−5056

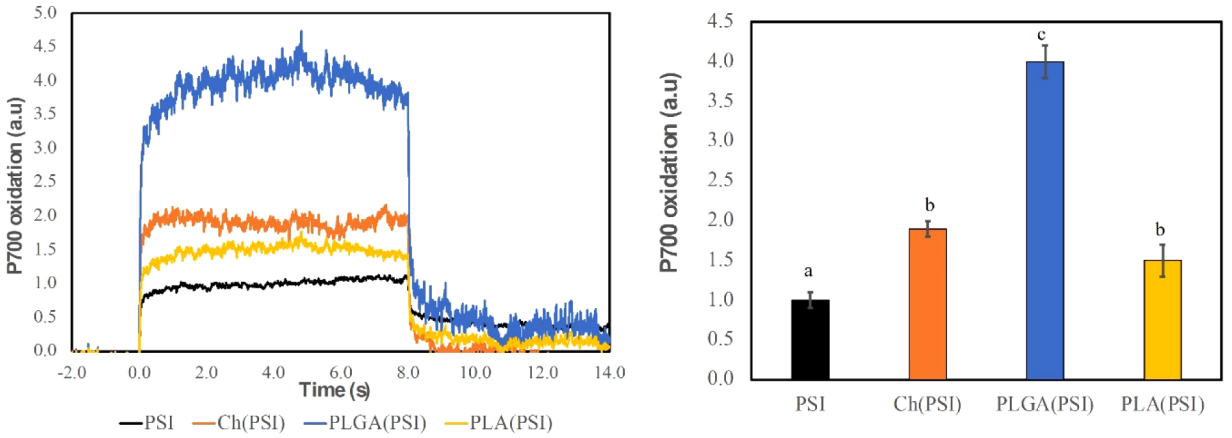

Figure 4. Photochemical activity of PSI. Light-dependent P700 oxidation of PSI in detergent or in biopolymer particles measured as transient absorption at 830 nm. Ascorbate and methyl-viologen were added as electron donor and acceptor, respectively. Red actinic light at 940 μmol m^{-2} s^{-1} was used to induce P700 oxidation. P700 oxidation kinetics were normalized to the chlorophyll content. All data were normalized to the P700 oxidation of the sample in the detergent (PSI black). Each experiment was performed in triplicate. Statistical significance is expressed by different letters according to the Tukey–Kramer test (n = 3).

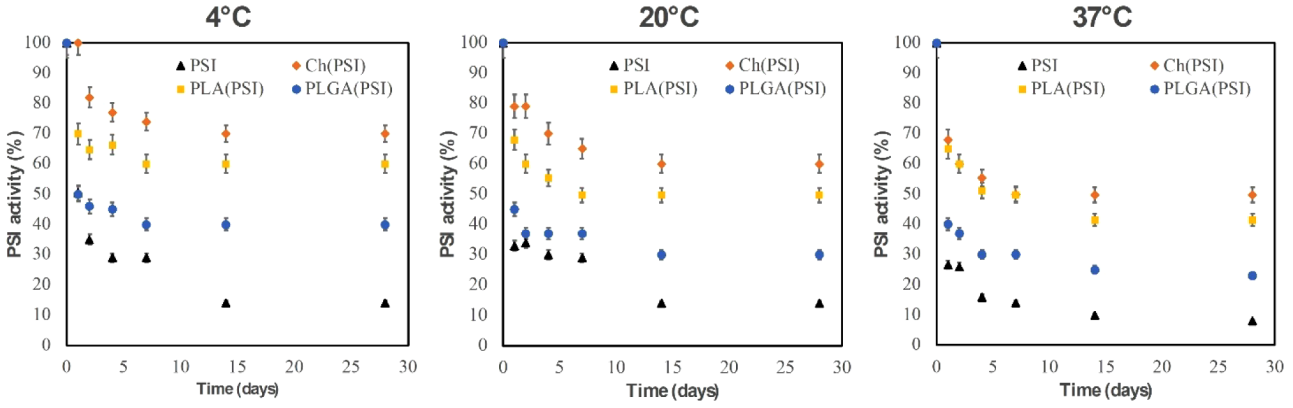

Figure 5. Photochemical activity of PSI, Ch(PSI), PLGA(PSI), and PLA(PSI) studied at different temperatures (4, 20, and 37 °C) over 30 days. The data are reported set to 100% at time 0. All the experiments were performed in triplicate. Data show p values < 0.05.

The encapsulation efficiency was then evaluated in terms of chlorophyll content by applying the equation reported in Materials and Methods. The higher EE of 89.6 ± 3.5% was obtained with PLA(PSI), while PLGA(PSI) and Ch(PSI) showed close values of 51.0 ± 0.5% and 46.3 ± 2.3%, respectively.

Photochemical Activity. The photochemical activity of PSI embedded within the biopolymers was compared to the activity measured from the same photosystem in a detergent solution. Upon normalization to the chlorophyll content, the highest P700 oxidation value was observed for PLGA(PSI), which was four times greater than that of PSI in the detergent solution. Nevertheless, each nanoformulation exhibited an increase in $P700^+$ formation compared to the same complex in detergent solution (Figure 4): 1.9 and 1.5 times for Ch(PSI) and PLA(PSI), respectively.

Due to the different properties in terms of size, charge surface, and composition, the influence of different pH levels (6, 7.4, 9) on the photochemical activities of PSI in detergent or in an organic matrix was investigated. The pH was adjusted by resuspending the samples in 10 mM citrate/NaOH, HEPES/NaOH, and glycine/NaOH buffers. The photochemical activity of Ch(PSI) and PLA(PSI) was not affected by pH in the range tested, while in the case of PLGA(PSI), the optimum pH for photochemical activity was 7.4.

Interestingly, at all pH levels tested, the photochemical activity of PSI in organic matrixes was higher than that of PSI in detergent solution (Table S2).

Stability of Photosystem I in Organic Matrix. The potential advantage of having a PSI complex encapsulated in an organic matrix is the increased stability due to the shell effect of the organic matrix.[13] Figure 5 shows the influence of different temperatures (4 °C, 20 °C, 37 °C) on the photochemical activity of free or encapsulated PSI upon incubation for up to 28 days. PSI in detergent solution was characterized by a strong reduction in photochemical activity, already reduced by 70% in less than 5 days at 4 °C and by 90% after 28 days at the same temperature. This decrease in PSI photochemical activity for PSI in detergent solution was even faster at increasing temperatures, with only 5% residual activity at 37 °C after 28 days. Generally, PSI embedded in biopolymers preserved activity longer than PSI in detergent (Figure 5). After 28 days, the relatively more preserved P700 activity was observed for Ch(PSI) with ∼ 20% decrease at 4 °C and ∼ 60% decrease at 37 °C, suggesting that chitosan could better preserve PSI activity than PLGA and PLA. PLGA(PSI) showed ∼ 40% decreased P700 activity at 4 °C and ∼ 25%

https://doi.org/10.1021/acssuschemeng.4c10593
ACS Sustainable Chem. Eng. 2025, 13, 5046−5056

decreased activity at 37 °C, while PLA(PSI) showed ∼ 65% at 4 °C and ∼ 50% at 37 °C decreased P700 activity.

The results reported in Figure 5 were obtained from samples stored in the dark. The influence of light on the stability of PSI was then evaluated by measuring the PSI photochemical activity after illumination with strong light (1,500 μmol $m^{-2}s^{-1}$) while maintaining the temperature at 4 °C. As reported in Figure 6, PSI in detergent solution almost

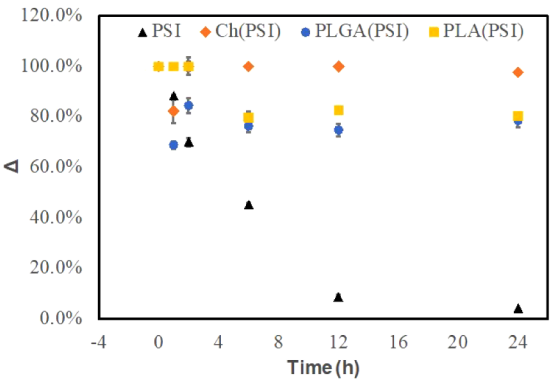

Figure 6. P700 oxidation kinetic of PSI, Ch(PSI), PLGA(PSI), and PLA(PSI) studied upon illumination with strong light (1,500 μmol $m^{-2}s^{-1}$) keeping the temperature at 4 °C. The data are reported set to 100% at time 0. All the experiments were performed in triplicate. Data show p values < 0.05.

completely lost its photochemical activity after 12 h of illumination. In contrast, PSI in PLGA, PLA, or Ch matrixes was much more stable. PSI in the chitosan matrix exhibited the highest stability of P700 activity, while both PLGA and PLA matrices preserved 80% of the PSI photochemical activity after 24 h of illumination.

Electron Transfer Reaction with External Electron Donor and Acceptor. The possibility of PSI in organic matrixes to catalyze light-dependent redox reactions was then investigated. PSI in the different organic matrixes was tested for the possible reduction of methylene blue (electron acceptor) using ascorbate as an electron donor. Methylene blue is commonly used as a redox indicator since its absorption in the 500−700 nm range decreases in the reduced form.[58] As reported in Figure 7, upon exposure to light, decreased methylene blue absorption was evident: even though decreased absorption of methylene blue was measured in the presence of empty nanoparticles, a much stronger decrease was evident in the presence of PSI, indicating the onset of a light-dependent redox reaction transferring electrons from ascorbate to methylene blue. Similar reduction efficiency of methylene blue was measured in the presence of different PSI complexes, in organic matrixes or in detergent solution, despite different photochemical efficiency for P700 reduction: these results suggest that the electron transfer from ascorbate to methylene blue is likely limited by the diffusion of the electron acceptor/donor in the nanoparticles.

The dependency of light-dependent electron transfer from ascorbate to methylene blue was then measured at different pH values and temperatures (Figure S6). The results obtained demonstrate that PLGA is the organic polymer inducing a stronger dependency on pH, according to the P700 oxidation measurements reported in Table S2. Regarding the temperature dependency, similar electron transfer efficiencies were measured at 4 or 20 °C for all samples, while a much lower reduction of methylene blue was measured at 37 °C, indicating a lower electron transfer efficiency at higher temperatures.

DISCUSSION

Membrane proteins can experience a decrease in stability and a loss of activity after purification steps due to changes in the environment in which they are embedded. In the case of photosynthetic proteins responsible for light harvesting and conversion, such as PSI, different photochemical activities have been reported when embedded in thylakoid membranes compared to isolated complexes. These issues may be caused by the leakage of proteins from the thylakoid membrane environment.[30] Even though PSI is the largest membrane protein complex with a known structure,[1] this does not ensure the ability to predict its future behavior when the complex is removed from its natural environment, and certain challenges

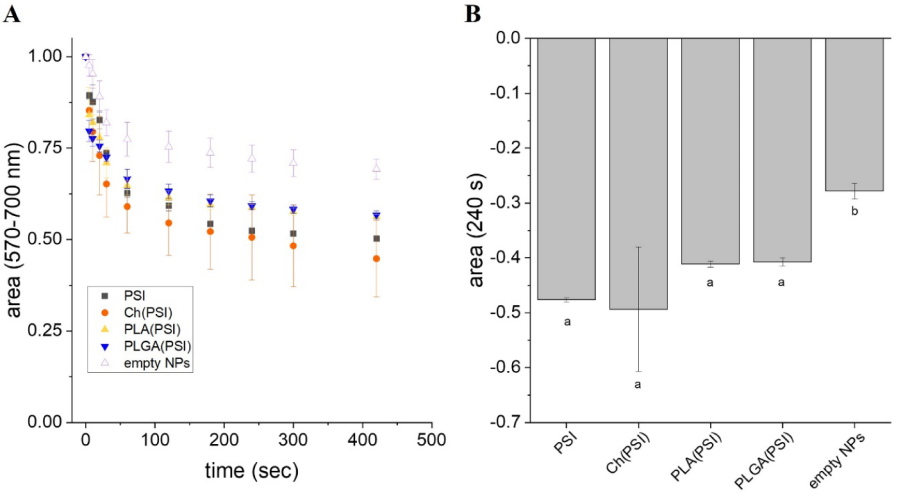

Figure 7. Light-dependent reduction of methylene blue. Samples were illuminated with blue light at 100 μmol m^{-2} s^{-1}. (A) Transient absorption data are reported as the difference in absorbance in the area between 570 and 700 nm, with the absorption value at time 0 set to 1. (B) Decreased absorption in the 570−700 nm area after 240 s of illumination. All the experiments were performed in triplicate. Errors bars represent standard deviation. Statistical significance is expressed by different letters according to the Tukey−Kramer test (n = 3).

https://doi.org/10.1021/acssuschemeng.4c10593
ACS Sustainable Chem. Eng. 2025, 13, 5046−5056

can arise from stabilization with detergents, making it prone to degradation. To achieve a more stable system over time, independent of the thylakoid membrane, nanotechnological supports can help address this problem.[59] In this article, we offer new advances in hybrid materials, featuring an efficient integration strategy of natural biopolymers and photosystem I. We developed a method to stabilize PSI in uniform, nonaggregated nanoassemblies, by embedding PSI with biopolymers, resulting in products within the nanometric range with a good PDI, indicative of monodispersity and homogeneity in the suspension.

We obtained three different nanoassemblies made from compatible biopolymers (chitosan, PLGA, and PLA) to address the issue of activity loss and provide a new environment to maintain the integrity of the photocatalytic system.[60,61] All three biopolymers are considered safe by both the EMA and FDA,[17,32−34,39] and the preparation protocols comply with the principles of green chemistry synthesis as the reactions are completed at room temperature and use nonhazardous materials; any solvents necessary for the reaction are considered safe at the concentrations used.

The increased photochemical activity of PSI in the different organic matrixes herein tested, compared to the detergent case, may result from enhanced protein−protein interactions that facilitate electron transfer and/or increased stability of the PSI complex upon encapsulation. Additionally, the protein interactions within organic matrixes may stabilize PSI in a more photochemically active state.

Encapsulation in PLGA and PLA broadened the absorption spectrum and increased emission above 720 nm compared to PSI in detergent (Figure 3B,C), consistent with previous data obtained using PSI from spinach embedded in a PLGA matrix (Cherubin et al. 2019). The enlargement of the absorption spectrum and increased emission at longer wavelengths suggest different protein−protein interactions in the embedded PSI complexes, likely causing stronger Chl-Chl interactions, which could enhance charge separation at the P700 reaction centers.

The spectroscopic results demonstrate that all nanoassemblies maintain their activity at different temperatures over time, while PSI in detergent degrades very quickly, even at 4 °C. As long as the purified and isolated PSI is kept in a detergent buffer, these conditions can affect the performance of the photosystem's catalytic center. During the activity test under strong light, the addition of electron acceptors and donors is necessary to verify the integrity of the photocatalytic process. For electron transfer, with PSI serving as the catalytic center, charge recombination is necessary to optimize the PSI-electrode interaction; during the free photosystem process, the gradient caused by the detergent can interfere with the activity of the carrier and also with the electron chain itself. Moreover, under this detergent-buffer condition, the PSI is not covered or inserted inside a double membrane environment that can mimic the thylakoid condition. In the case of nanoassemblies embedding PSI, the advantages are significant for all nanoformulations (PLGA, PLA, and Ch): PSI is stable at different temperatures and functions in different conditions, thanks to the protective shell provided by the organic polymers.[13] We investigated the resilience of embedded PSI in different pH conditions and found similar P700 activity from pH 6 to 9 when PSI was embedded in PLA or Ch matrixes, while the highest photochemical activity was observed at pH 7.4 with PLGA. Interestingly, even though the activity decreased compared to pH 7.4, the P700 activity of PSI in PLGA matrices at pH 6 or pH 9 was higher compared to any other PSI sample under any conditions tested herein.

The most interesting results are related to the ability of PSI in an organic matrix to keep the electron reaction chain functioning: it is worth mentioning that the nanosystems retain up to 7- to 8-fold greater activity when compared to PSI in detergent during 28 days of testing, depending on the nanomaterial considered.

Light-dependent electron transfer reactions could be obtained ex vivo by using an artificial electron donor (ascorbate) and acceptor (methylene blue) catalyzed by PSI in organic nanoparticles (Figure 7). Similar electron transfer efficiency observed across different sample analyses, despite variations in P700 oxidation refineries, suggests that the diffusion of electron acceptors or donors within the microparticles is likely limiting the light-dependent redox reactions. PLGA samples exhibited a stronger dependency on pH for the catalysis of electron transfer reactions, consistent with the P700 oxidation measurements (Table S2). It is worth noting that PLGA matrixes were previously reported as being sensitive to different pH levels, with destabilization of PLGA polymers occurring at acidic pH or at pH ∼ 9.[62] It is also worth noting that the P700 oxidation measurements lasted 8 s (Figure 4) and consistently, after 10 s, the best electron transfer efficiency from ascorbate to methylene blue was measured at pH 7.4 for the PLGA sample. On a longer time scale, the condition at pH 6 was the most efficient in terms of electron transport; this could be related to the partial disassembly of PLGA polymers at lower pH, allowing more efficient diffusion of the electron donor/acceptor to interact with PSI. Regarding temperature dependency, similar electron transfer efficiencies were measured at 4 or 20 °C, while a significantly lower reduction of methylene blue was measured at 37 °C. Due to the short exposure of PSI samples to these temperatures, the results obtained are likely not related to the stability of the complex at these temperatures but are more likely related to the increasing dynamics of the polymers at higher temperatures, which reduced the efficiency of the interaction between PSI and the electron donor and/or electron acceptor, thereby decreasing the electron transfer efficiency. Additional work is required to assess the dynamics of proteins and organic polymers at different temperatures.

Compared to previous findings on PSI isolated from plants embedded in a PLGA matrix,[13] this study successfully demonstrated the isolation and incorporation of different organic matrixes of PSI isolated from the green alga *C. reinhardtii*. The use of microalgae for PSI isolation avoids competition with food applications, unlike the use of spinach leaves, for instance. *C. reinhardtii* does not require arable land for cultivation, and in general, the carbon and water footprints associated with microalgae cultivation are more favorable compared to land plant cultivation.[63,64] Moreover, the biomass productivity of microalgae has been reported to be potentially higher per unit of available surface compared with land plants. Here, the positive effect of PLGA in stabilizing PSI and improving P700 activity was confirmed, as observed in previous findings using PSI isolated from plants.[13] However, here, other organic matrices were successfully tested, further improving the stability and activity of PSI, as PLA and Ch. Surprisingly, Ch emerged as the organic matrix with the highest efficiency in stabilizing PSI activity over time, at different temperatures and under exposure to strong light. Compared to previous work (Cherubin et al., 2019), the

https://doi.org/10.1021/acssuschemeng.4c10593
ACS Sustainable Chem. Eng. 2025, 13, 5046−5056

particle sizes were significantly reduced, leading to an increased surface area, which resulted in improved photochemical activity of PSI. The advantages of the technology proposed herein open a new frontier for the use of nanosystems as enhanced antennas and stability supports for the photocatalytic activity of PSI. These nanosystems can be easily integrated into devices or used independently for light-to-electron conversion purposes, ranging from in vitro photochemical reactions to organic and environmentally friendly photovoltaic devices or the photoactivation of mammalian cells, leveraging the larger surface area and the different surface charge properties.

CONCLUSIONS

In conclusion, in this work, we gave a proof of concept for the stabilization of extracellular photosystems using biocompatible and biodegradable nanoparticles to exploit their ex vivo photocatalytic capabilities. Interestingly, the nanoencapsulation procedure does not affect the ability of PSI to transfer electrons but significantly increases its activity, probably providing a stable environment in comparison to the photosystem in detergents. The results obtained have potentially useful applications, including (1) the production of hydrogen by light-driven water splitting, (2) proton-driven catalytic reactions, and (3) the production of hydride nano/micro architectures for electric conduction.

ASSOCIATED CONTENT

Supporting Information

The Supporting Information is available free of charge at https://pubs.acs.org/doi/10.1021/acssuschemeng.4c10593.

ζ-potential value of empty and loaded nanoparticles (Table S1); photochemical activity of PSI, Ch(PSI), PLGA(PSI), and PLA(PSI) studied at different pH levels (6, 7.4, and 9) (Table S2); photosystem I isolation (Figure S1); PSI encapsulation in chitosan MPs (Figure S2); PSI encapsulation in PLGA and PLA MPs (Figure S3); photosystem I encapsulation (Figure S4); SDS-PAGE of photosystem I before and after encapsulation in organic matrixes (Figure S5); and electron transfer analysis at different pH and temperature values (Figure S6) (PDF)

AUTHOR INFORMATION

Corresponding Authors

Matteo Ballottari − *Department of Biotechnology, University of Verona, Verona 37134, Italy;* orcid.org/0000-0001-8410-3397; Phone: +39-0458027823; Email: matteo.ballottari@univr.it

Massimiliano Perduca − *Department of Biotechnology, University of Verona, Verona 37134, Italy;* orcid.org/0000-0001-8291-0523; Phone: +39-0458027984; Email: massimiliano.perduca@univr.it

Authors

Salvatore C. Gaglio − *Department of Biotechnology, University of Verona, Verona 37134, Italy*

Giorgia Zanella − *Department of Biotechnology, University of Verona, Verona 37134, Italy*

Stefano Cazzaniga − *Department of Biotechnology, University of Verona, Verona 37134, Italy;* orcid.org/0000-0002-2824-7916

Nico Olivieri − *Department of Biotechnology, University of Verona, Verona 37134, Italy*

Elia Battagini − *Department of Biotechnology, University of Verona, Verona 37134, Italy*

Alessandro Romeo − *Department of Computer Science, University of Verona, Verona 37134, Italy;* orcid.org/0000-0001-5068-8788

Complete contact information is available at: https://pubs.acs.org/10.1021/acssuschemeng.4c10593

Author Contributions

#S.C.G. and G.Z. contributed equally as co-first authors. M.P. and M.B. conceived the work; M.P. supervised the nanoparticle synthesis; M.B. supervised the purification and spectroscopic characterization of PSI; S.C.G. and G.Z. performed the nanoparticle synthesis and characterization; S.C.G., G.Z., and S.C. performed the P700 oxidation analysis; N.O., E.B., and S.C. performed the experiments reported in Figure 7, Figure S5, and Figure S6. M.P., M.B., S.C.G., G.Z., and S.C. wrote the paper; all the authors discussed the results and commented on the manuscript.

Funding

This research was funded by the FUR (Fondo Unico della Ricerca-University of Verona) of M. Perduca and M. Ballottari.

Notes

The authors declare no competing financial interest.

ACKNOWLEDGMENTS

The authors gratefully thank the facility "Centro Piattaforme Tecnologiche" of the University of Verona for access to the Nano Zeta Sizer ZS, ZEN3600 (Malvern Instruments, Malvern, Worcestershire, United Kingdom) and the Malvern NanoSight NS300 instrument (Worcestershire, UK).

ABBREVIATIONS

PSI, photosystem I; PSII, photosystem II; PLGA, poly lactic-co-glycolic acid; PLA, poly lactic acid; Ch, chitosan; MPs, microparticles; AFM, atomic force microscopy; DSC, differential scanning calorimetry; FDA, US Food and Drug Administration; EMA, European Medicines Agency; TPP, tripolyphosphate; PVA, poly(vinyl alcohol); DLS, dynamic light scattering; Chl, chlorophylls

REFERENCES

(1) Ben-Shem, A.; Frolow, F.; Nelson, N. Crystal Structure of Plant Photosystem I. *Nature* **2003**, *426* (6967), 630−635.

(2) Qin, X.; Suga, M.; Kuang, T.; Shen, J.-R. Structural Basis for Energy Transfer Pathways in the Plant PSI-LHCI Supercomplex. *Science* **2015**, *348* (6238), 989−995.

(3) Rochaix, J.-D. *Chlamydomonas*, a Model System for Studying the Assembly and Dynamics of Photosynthetic Complexes. *FEBS Lett.* **2002**, *529* (1), 34−38.

(4) Häder, D.-P. Photosynthesis in Plants and Algae. *Anticancer Res.* **2022**, *42* (10), 5035−5041.

(5) Mazor, Y.; Borovikova, A.; Nelson, N. The Structure of Plant Photosystem I Super-Complex at 2.8 Å Resolution. *eLife* **2015**, *4*, No. e07433.

(6) Izzo, M.; Jacquet, M.; Fujiwara, T.; Harputlu, E.; Mazur, R.; Wróbel, P.; Góral, T.; Unlu, C. G.; Ocakoglu, K.; Miyagishima, S.; Kargul, J. Development of a Novel Nanoarchitecture of the Robust Photosystem I from a Volcanic Microalga Cyanidioschyzon Merolae on Single Layer Graphene for Improved Photocurrent Generation. *Int. J. Mol. Sci.* **2021**, *22* (16), 8396.

(7) Frolov, L.; Rosenwaks, Y.; Carmeli, C.; Carmeli, I. Fabrication of a Photoelectronic Device by Direct Chemical Binding of the Photosynthetic Reaction Center Protein to Metal Surfaces. *Adv. Mater.* **2005**, *17* (20), 2434−2437.
(8) Kaniber, S. M.; Simmel, F. C.; Holleitner, A. W.; Carmeli, I. The Optoelectronic Properties of a Photosystem I−Carbon Nanotube Hybrid System. *Nanotechnology* **2009**, *20* (34), 345701.
(9) Krassen, H.; Schwarze, A.; Friedrich, B.; Ataka, K.; Lenz, O.; Heberle, J. Photosynthetic Hydrogen Production by a Hybrid Complex of Photosystem I and [NiFe]-Hydrogenase. *ACS Nano* **2009**, *3* (12), 4055−4061.
(10) Kawahara, K.; Inoue-Kahino, N.; Namie, K.; Kato, Y.; Tomo, T.; Shibata, Y.; Kashino, Y.; Noguchi, T. A Gold Nanoparticle Conjugate with Photosystem I and Photosystem II for Development of a Biohybrid Water-Splitting Photocatalyst. *Biomed. Spectrosc. Imaging* **2020**, *9* (1−2), 73−81.
(11) Saboe, P. O.; Conte, E.; Farell, M.; Bazan, G. C.; Kumar, M. Biomimetic and Bioinspired Approaches for Wiring Enzymes to Electrode Interfaces. *Energy Environ. Sci.* **2017**, *10* (1), 14−42.
(12) Saboe, P. O.; Conte, E.; Chan, S.; Feroz, H.; Ferlez, B.; Farell, M.; Poyton, M. F.; Sines, I. T.; Yan, H.; Bazan, G. C.; Golbeck, J.; Kumar, M. Biomimetic Wiring and Stabilization of Photosynthetic Membrane Proteins with Block Copolymer Interfaces. *J. Mater. Chem. A* **2016**, *4* (40), 15457−15463.
(13) Cherubin, A.; Destefanis, L.; Bovi, M.; Perozeni, F.; Bargigia, I.; de la Cruz Valbuena, G.; D'Andrea, C.; Romeo, A.; Ballottari, M.; Perduca, M. Encapsulation of Photosystem I in Organic Microparticles Increases Its Photochemical Activity and Stability for Ex Vivo Photocatalysis. *ACS Sustainable Chem. Eng.* **2019**, *7* (12), 10435−10444.
(14) Hwang, E. T.; Gu, M. B. Enzyme Stabilization by Nano/Microsized Hybrid Materials: Enzyme Stabilization by Nano/Microsized Hybrid Materials. *Eng. Life Sci.* **2013**, *13* (1), 49−61.
(15) Weng, Y.; Ranaweera, S.; Zou, D.; Cameron, A. P.; Chen, X.; Song, H.; Zhao, C.-X. Improved Enzyme Thermal Stability, Loading and Bioavailability Using Alginate Encapsulation. *Food Hydrocolloids* **2023**, *137*, 108385.
(16) Ma, G. Microencapsulation of Protein Drugs for Drug Delivery: Strategy, Preparation, and Applications. *J. Controlled Release* **2014**, *193*, 324−340.
(17) Batool, I.; Iqbal, A.; Imran, M.; Ramzan, M.; Anwar, A. Design and Applications of Enzyme-Linked Nanostructured Materials for Efficient Bio-Catalysis. *Top. Catal.* **2023**, *66*, 649.
(18) Malferrari, M.; Savitsky, A.; Mamedov, M. D.; Milanovsky, G. E.; Lubitz, W.; Möbius, K.; Semenov, A. Y.; Venturoli, G. Trehalose Matrix Effects on Charge-Recombination Kinetics in Photosystem I of Oxygenic Photosynthesis at Different Dehydration Levels. *Biochim. Biophys. Acta, Bioenerg.* **2016**, *1857* (9), 1440−1454.
(19) Niroomand, H.; Mukherjee, D.; Khomami, B. Tuning the Photoexcitation Response of Cyanobacterial Photosystem I via Reconstitution into Proteoliposomes. *Sci. Rep.* **2017**, *7* (1), 2492.
(20) Joly, D.; Govindachary, S.; Fragata, M. Photosystem II Reconstitution into Proteoliposomes and Methodologies for Structure−Function Characterization. In *Photosynthesis Research Protocols*, Carpentier, R., Ed.; Humana Press: Totowa, NJ, 2011; Vol. *684*; pp. 217−245. DOI: .
(21) Kaniber, S. M.; Brandstetter, M.; Simmel, F. C.; Carmeli, I.; Holleitner, A. W. On-Chip Functionalization of Carbon Nanotubes with Photosystem I. *J. Am. Chem. Soc.* **2010**, *132* (9), 2872−2873.
(22) Mershin, A.; Matsumoto, K.; Kaiser, L.; Yu, D.; Vaughn, M.; Nazeeruddin, M. K.; Bruce, B. D.; Graetzel, M.; Zhang, S. Self-Assembled Photosystem-I Biophotovoltaics on Nanostructured TiO2 and ZnO. *Sci. Rep.* **2012**, *2* (1), 234.
(23) Pamu, R.; Sandireddy, V. P.; Kalyanaraman, R.; Khomami, B.; Mukherjee, D. Plasmon-Enhanced Photocurrent from Photosystem I Assembled on Ag Nanopyramids. *J. Phys. Chem. Lett.* **2018**, *9* (5), 970−977.
(24) Hussels, M.; Nieder, J. B. Interactions of Photosystem I with Plasmonic Nanostructures. *Acta Phys. Pol., A* **2012**, *122* (2), 269−274.
(25) Czechowski, N.; Lokstein, H.; Kowalska, D.; Ashraf, K.; Cogdell, R. J.; Mackowski, S. Large Plasmonic Fluorescence Enhancement of Cyanobacterial Photosystem I Coupled to Silver Island Films. *Appl. Phys. Lett.* **2014**, *105* (4), 043701.
(26) Robinson, M. T.; Simons, C. E.; Cliffel, D. E.; Jennings, G. K. Photocatalytic Photosystem I/PEDOT Composite Films Prepared by Vapor-Phase Polymerization. *Nanoscale* **2017**, *9* (18), 6158−6166.
(27) Badura, A.; Guschin, D.; Kothe, T.; Kopczak, M. J.; Schuhmann, W.; Rögner, M. Photocurrent Generation by Photosystem 1 Integrated in Crosslinked Redox Hydrogels. *Energy Environ. Sci.* **2011**, *4* (7), 2435.
(28) Carmeli, I.; Frolov, L.; Carmeli, C.; Richter, S. Photovoltaic Activity of Photosystem I-Based Self-Assembled Monolayer. *J. Am. Chem. Soc.* **2007**, *129* (41), 12352−12353.
(29) Gerster, D.; Reichert, J.; Bi, H.; Barth, J. V.; Kaniber, S. M.; Holleitner, A. W.; Visoly-Fisher, I.; Sergani, S.; Carmeli, I. Photocurrent of a Single Photosynthetic Protein. *Nat. Nanotechnol.* **2012**, *7* (10), 673−676.
(30) Teodor, A. H.; Thal, L. B.; Vijayakumar, S.; Chan, M.; Little, G.; Bruce, B. D. Photosystem I Integrated into Mesoporous Microspheres Has Enhanced Stability and Photoactivity in Biohybrid Solar Cells. *Mater. Today Bio* **2021**, *11*, 100122.
(31) Mahata, C.; Das, P.; Khan, S.; Thaher, M. I. A.; Abdul Quadir, M.; Annamalai, S. N.; Al Jabri, H. The Potential of Marine Microalgae for the Production of Food, Feed, and Fuel (3F). *Fermentation* **2022**, *8* (7), 316.
(32) Danhier, F.; Ansorena, E.; Silva, J. M.; Coco, R.; Le Breton, A.; Préat, V. PLGA-Based Nanoparticles: An Overview of Biomedical Applications. *J. Controlled Release* **2012**, *161* (2), 505−522.
(33) Casalini, T.; Rossi, F.; Castrovinci, A.; Perale, G. A Perspective on Polylactic Acid-Based Polymers Use for Nanoparticles Synthesis and Applications. *Front. Bioeng. Biotechnol.* **2019**, *7*, 259.
(34) Tyler, B.; Gullotti, D.; Mangraviti, A.; Utsuki, T.; Brem, H. Polylactic Acid (PLA) Controlled Delivery Carriers for Biomedical Applications. *Adv. Drug Delivery Rev.* **2016**, *107*, 163−175.
(35) Herdiana, Y.; Wathoni, N.; Shamsuddin, S.; Muchtaridi, M. Drug Release Study of the Chitosan-Based Nanoparticles. *Heliyon* **2022**, *8* (1), No. e08674.
(36) Farah, S.; Anderson, D. G.; Langer, R. Physical and Mechanical Properties of PLA, and Their Functions in Widespread Applications — A Comprehensive Review. *Adv. Drug Delivery Rev.* **2016**, *107*, 367−392.
(37) Park, T. G. Degradation of Poly(Lactic-Co-Glycolic Acid) Microspheres: Effect of Copolymer Composition. *Biomaterials* **1995**, *16* (15), 1123−1130.
(38) Walker, J.; Albert, J.; Liang, D.; Sun, J.; Schutzman, R.; Kumar, R.; White, C.; Beck-Broichsitter, M.; Schwendeman, S. P. In Vitro Degradation and Erosion Behavior of Commercial PLGAs Used for Controlled Drug Delivery. *Drug Delivery Transl. Res.* **2023**, *13* (1), 237−251.
(39) Naskar, S.; Sharma, S.; Kuotsu, K. Chitosan-Based Nanoparticles: An Overview of Biomedical Applications and Its Preparation. *J. Drug Delivery Sci. Technol.* **2019**, *49*, 66−81.
(40) Chowdhury, M. S.; Oliullah, M. S.; Islam, R. T.; Hurayra, M. A.; Mahmud, M. Z. A.; Hasan, N.; Rahman, M. K.; Islam, M. S.; Khan, J.; Hossain, N. Biomaterials for Energy Storage: Synthesis, Properties, and Performance. *Green Technol. Sustainability* **2025**, *3* (2), 100152.
(41) Lan, G.; Fan, Y.; Shi, W.; You, E.; Veroneau, S. S.; Lin, W. Biomimetic Active Sites on Monolayered Metal−Organic Frameworks for Artificial Photosynthesis. *Nat. Catal.* **2022**, *5* (11), 1006−1018.
(42) Martins, C.; Sousa, F.; Araújo, F.; Sarmento, B. Functionalizing PLGA and PLGA Derivatives for Drug Delivery and Tissue Regeneration Applications. *Adv. Healthcare Mater.* **2018**, *7* (1), 1701035.
(43) Jhaveri, J.; Raichura, Z.; Khan, T.; Momin, M.; Omri, A. Chitosan Nanoparticles-Insight into Properties, Functionalization and Applications in Drug Delivery and Theranostics. *Molecules* **2021**, *26* (2), 272.

https://doi.org/10.1021/acssuschemeng.4c10593
ACS Sustainable Chem. Eng. 2025, 13, 5046−5056

(44) Haddad, T.; Noel, S.; Liberelle, B.; El Ayoubi, R.; Ajji, A.; De Crescenzo, G. Fabrication and Surface Modification of Poly Lactic Acid (PLA) Scaffolds with Epidermal Growth Factor for Neural Tissue Engineering. *Biomatter* **2016**, *6* (1), No. e1231276.
(45) Thauvin, C.; Schwarz, B.; Delie, F.; Allémann, E. Functionalized PLA Polymers to Control Loading and/or Release Properties of Drug-Loaded Nanoparticles. *Int. J. Pharm.* **2018**, *548* (2), 771−777.
(46) Kropat, J.; Hong-Hermesdorf, A.; Casero, D.; Ent, P.; Castruita, M.; Pellegrini, M.; Merchant, S. S.; Malasarn, D. A Revised Mineral Nutrient Supplement Increases Biomass and Growth Rate in *Chlamydomonas Reinhardtii*. *Plant J.* **2011**, *66* (5), 770−780.
(47) McCall, R. L.; Sirianni, R. W. PLGA Nanoparticles Formed by Single- or Double-Emulsion with Vitamin E-TPGS. *J. Visualized Exp.* **2013**, No. 82, 51015.
(48) Pinon-Segundo, E.; Nava-Arzaluz, M. G.; Lechuga-Ballesteros, D. Pharmaceutical Polymeric Nanoparticles Prepared by the Double Emulsion- Solvent Evaporation Technique. *Recent Pat. CNS Drug Discovery* **2012**, *6* (3), 224−235.
(49) Pulingam, T.; Foroozandeh, P.; Chuah, J.-A.; Sudesh, K. Exploring Various Techniques for the Chemical and Biological Synthesis of Polymeric Nanoparticles. *Nanomaterials* **2022**, *12* (3), 576.
(50) Stetefeld, J.; McKenna, S. A.; Patel, T. R. Dynamic Light Scattering: A Practical Guide and Applications in Biomedical Sciences. *Biophys. Rev.* **2016**, *8* (4), 409−427.
(51) Knysh, A.; Sokolov, P.; Nabiev, I. Dynamic Light Scattering Analysis in Biomedical Research and Applications of Nanoparticles and Polymers. *J. Biomed. Photonics Eng.* **2023**, 020203.
(52) Filipe, V.; Hawe, A.; Jiskoot, W. Critical Evaluation of Nanoparticle Tracking Analysis (NTA) by NanoSight for the Measurement of Nanoparticles and Protein Aggregates. *Pharm. Res.* **2010**, *27* (5), 796−810.
(53) Nguyen-Tri, P.; Ghassemi, P.; Carriere, P.; Nanda, S.; Assadi, A. A.; Nguyen, D. D. Recent Applications of Advanced Atomic Force Microscopy in Polymer Science: A Review. *Polymers* **2020**, *12* (5), 1142.
(54) Averina, S. G.; Velichko, N. V.; Pinevich, A. A.; Senatskaya, E. V.; Pinevich, A. V. Non-a Chlorophylls in Cyanobacteria. *Photosynthetica* **2019**, *57* (4), 1109−1118.
(55) Chazaux, M.; Schiphorst, C.; Lazzari, G.; Caffarri, S. Precise Estimation of Chlorophyll *a*, *b* and Carotenoid Content by Deconvolution of the Absorption Spectrum and New Simultaneous Equations for Chl Determination. *Plant J.* **2022**, *109* (6), 1630−1648.
(56) Le Quiniou, C.; Tian, L.; Drop, B.; Wientjes, E.; Van Stokkum, I. H. M.; Van Oort, B.; Croce, R. PSI−LHCI of *Chlamydomonas Reinhardtii*: Increasing the Absorption Cross Section without Losing Efficiency. *Biochim. Biophys. Acta, Bioenerg.* **2015**, *1847* (4−5), 458−467.
(57) Croce, R.; Dorra, D.; Holzwarth, A. R.; Jennings, R. C. Fluorescence Decay and Spectral Evolution in Intact Photosystem I of Higher Plants. *Biochemistry* **2000**, *39* (21), 6341−6348.
(58) Edison, T. J. I.; Sethuraman, M. G. Instant Green Synthesis of Silver Nanoparticles Using Terminalia Chebula Fruit Extract and Evaluation of Their Catalytic Activity on Reduction of Methylene Blue. *Process Biochem.* **2012**, *47* (9), 1351−1357.
(59) Yoon, J.; Shin, M.; Lim, J.; Kim, D. Y.; Lee, T.; Choi, J. Nanobiohybrid Material-Based Bioelectronic Devices. *Biotechnol. J.* **2020**, *15* (6), 1900347.
(60) Teodor, A. H.; Bruce, B. D. Putting Photosystem I to Work: Truly Green Energy. *Trends Biotechnol.* **2020**, *38* (12), 1329−1342.
(61) Anozie, U. C.; Dalhaimer, P. Molecular Links among Non-Biodegradable Nanoparticles, Reactive Oxygen Species, and Autophagy. *Adv. Drug Delivery Rev.* **2017**, *122*, 65−73.
(62) Witschi, C.; Doelker, E. Influence of the Microencapsulation Method and Peptide Loading on Poly(Lactic Acid) and Poly(Lactic-Co-Glycolic Acid) Degradation during in Vitro Testing. *J. Controlled Release* **1998**, *51* (2−3), 327−341.
(63) Pugazhendhi, A.; Nagappan, S.; Bhosale, R. R.; Tsai, P.-C.; Natarajan, S.; Devendran, S.; Al-Haj, L.; Ponnusamy, V. K.; Kumar, G. Various Potential Techniques to Reduce the Water Footprint of Microalgal Biomass Production for Biofuel—A Review. *Sci. Total Environ.* **2020**, *749*, 142218.
(64) Chen, Y.; You, L.; Sun-Waterhouse, D. Effects of Processing on the Physicochemical Characteristics and Health Benefits of Algae Products: Trade-Offs among Food Carbon Footprint Nutrient Profiles, Health Properties, and Consumer Acceptance. *Trends Food Sci. Technol.* **2024**, *147*, 104375.

https://doi.org/10.1021/acssuschemeng.4c10593
ACS Sustainable Chem. Eng. 2025, 13, 5046−5056